Stability Analysis of Boundary Layer Flow and Heat Transfer of Fe_2O_3 and Fe-Water Base Nanofluid over a Stretching/Shrinking Sheet with Radiation Effect

Hazoor Bux Lanjwani
Institute of Mathematics and Computer Science
University of Sindh
Jamshoro, Pakistan
hazoor.bux@scholars.usindh.edu.pk

Muhammad Saleem Chandio
Institute of Mathematics and Computer Science
University of Sindh
Jamshoro, Pakistan
mschandio@hotmail.com

Kamran Malik
Department of Mathematics
Government College University
Hyderabad, Pakistan
Kamranmk99@gmail.com

Muhammad Mujtaba Shaikh
Department of Basic Sciences and Related Studies
Mehran University of Engineering and Technology
Jamshoro, Pakistan
mujtaba.shaikh@faculty.muet.edu.pk

Abstract-In this paper, the radiation and slip effects are investigated on the boundary layer flow and heat transfer of Fe_2O_3 and Fe-water base nanofluids over a porous stretching/shrinking sheet. A similarity transformation is used to convert the system of governing partial differential equations into ordinary differential equations, which are then numerically solved in Maple software with the help of the shooting technique. At different ranges of the applied parameters, dual solutions are found. The effects of the different physical factors such as radiation, nanoparticle volumetric fractions, suction, and slip parameters are determined and discussed. The skin-friction coefficient and local Nusselt number are influenced significantly by the applied parameters. In the boundary layer regime, the increase in nanoparticle volume fractions and radiation parameters enhance the temperature and boundary-layer thicknesses, while increasing Prandtl number, suction, and thermal slip parameters decrease the temperature and reduce thermal boundary-layer thicknesses. The suspension of iron nanoparticles shows more enhancement in skin friction and Nusselt number than the iron oxide nanoparticles in base fluid water.

Keywords-boundary layer; dual solutions; shooting method; rediation; nanofluid

I. INTRODUCTION

Nanofluids are made up of solid nanoparticles and common base fluids such as water, oil, glycol, polymer fluids, and so on [1, 3-5]. The nanoparticles are made from metals, metal oxides, and carbides, and have far greater heat conductivity. Their insertion considerably enhances thermo-physical properties such as thermal conductivity, viscosity, thermal diffusivity, and the convective heat transfer coefficient. Nanofluids may be employed in many industrial and technological applications [2], including microelectronics, coolants, fuel cells, pharmaceutical operations, household freezers, chillers, and lubricants. Several methods have been developed to improve the thermal conductivity of typical common liquids, including suspending macro/micro particles of solid materials in them.

Two types of nanofluid modelshave been created and effectively employed as a result of recent developments in nanotechnology. Buongiorno [6] proposed the initial model, which incorporated 7 slip factors as critical components in generating a relative velocity between the nanoparticles and the base fluid. Only thermophoresis and Brownian motion were considered essential among the 7 slip components when creating a model for convective transport in nanofluids. The second nanofluid model was proposed by Tiwari and Das [7] to study the effect of nanoparticle volume fractions on thermal characteristics enhancement. Researchers used and modified these two well-known nanofluid models by using different physical flow parameters [8-11].

Many engineering and practical science applications, such as paper manufacturing, wire drawing, extrusion, metal spinning, and hot rolling, rely on the boundary layer flow through a stretching/shrinking sheet. Crane [12] was the first to work on the stretched sheet. Since then, a broad range of issues related to these topics was examined. Authors in [13] examined the heat and mass transfer on a stretched sheet with suction and blowing. Many researchers were also interested to study the flow over a stretching sheet. The study of viscous flow past on shrinking sheet along the suction action was pioneered in [14]. It is worth mentioning that mass suction is required to keep the flow inside boundary layer flowing. The analytic solution of the magnetohydrodynamic flow of a second grade fluid on a shrinking sheet was investigated in [15]. Authors in [16] explored the MHD rotational flow of a viscous fluid over a

Corresponding author: Muhammad Mujtaba Shaikh

shrinking surface. Authors in [17] were the first to investigate the nanofluid flow through the boundary layer of a stretching sheet. The boundary layer slip flow problem is quite relevant in practice. Wang [18] analyzed the impact of the partial slip on flow of a viscous fluid through a stretching sheet using numerical simulations. Authors in [19] examined the natural convection of magnetohydrodynamics nanofluid flow on a vertically flat plate. Authors in [20] examined the impact of the particle sizes and volume fractions on the Al_2O_3-water base nanofluid. Authors in [21] studied the steady boundary-layer flow through a continuously moving plate with different nanoparticles immersed in water in a 2D (two-dimensional) flow. Author in [22] considered 2D nanofluid flow past a moving plate in a continuous free-stream. Authors in [23] examined 2D laminar stagnant-point fluid flow with heat absorption and generation. Authors in [24] investigated the behavior of slip factors using single and multiphase nanomaterial models. Authors in [25] inspected the inclination of the magnetic field in a convective radiative heat transfer micro-nanofluid using a porous medium.

Various scholars have studied the occurrence of multiple solutions to the boundary value problems. These solutions are caused by the non-linearity of the equations at various ranges of the physical parameters that can be seen in the literature. Several academics assessed the stability of a range of solutions to find which is the stable and physically realizable. Many scholars, including the authors in [26-28] have come up with different solutions and they proved that only one solution was found stable through stability analysis.

The primary aim of this study is to determine how various flow parameters impact water-based nanofluids created by stretching and shrinking sheets. The Tiwari and Das model is used to investigate the heat radiation and slip effects of iron (Fe) and iron oxide (Fe_2O_3) nanoparticles. The similarity transformations are used to convert the partial differential equations into ordinary differential equations,. The shooting approach is applied for solution of the resulting system of equations. According to the findings of this study, dual solutions exist for certain ranges of the physical parameters that are illustrated in the graphs. Due to the occurrence of dual solutions, the bvp4c Matlab program is used to perform the stability analysis. The stability tests reveal that the first solution is the stable and the physically realizable, while the second is not stable.

II. PROBLEM FORMULATION

Let's consider a two-dimensional boundary layer flow and heat transfer in a water-based nanofluid containing iron (Fe) and iron oxide (Fe_2O_3) nanoparticles over a stretching/ shrinking sheet. The sheet is considered to be parallel to the plane $y = 0$, and the flow is contained at $y > 0$. The sheet is stretched and shrunk with velocity $u_w = cx$, where $c > 0$ is the stretching rate, with two opposed and equal forces applied in the direction of the x-axis. The base fluid (water) and nanoparticles are considered to be in thermal equilibrium. Table I lists the thermo physical properties of water as well as the nanoparticles that are used in the present study.

TABLE I. THERMO PHYSICAL VALUES OF BASE-FLUID AND SOLID NANOPARTICLES [36]

Base fluid and kind of particles	$\rho(kg/m^3)$	$C_p(J/Kgk)$	$k(W/mk)$
Water (H_2O)	997.1	4179	0.613
Iron (Fe)	7870	460	80
Iron oxide (Fe_2O_3)	5180	670	80.4

The governing equations of the problem by using the Tiwari and Das model [7] are written as:

$$\frac{\partial v}{\partial y} + \frac{\partial u}{\partial x} = 0 \quad (1)$$

$$v\frac{\partial u}{\partial y} + u\frac{\partial u}{\partial x} = \frac{\mu_{nf}}{\rho_{nf}}\frac{\partial^2 u}{\partial y^2} \quad (2)$$

$$v\frac{\partial T}{\partial y} + u\frac{\partial T}{\partial x} = \alpha_{nf}\frac{\partial^2 T}{\partial y^2} - \frac{1}{(\rho c_p)_{nf}}\frac{\partial q_r}{\partial y} \quad (3)$$

The Roseland approximation, q_r is defined as:

$$q_r = -\frac{4\sigma^*}{3k^*}\frac{\partial T^4}{\partial y} \quad (4)$$

where σ^* is Boltzmann's constant and k* is the absorption coefficient. It is assumed that the temperature difference is very small. As a result, when the Taylor series is applied to the temperature of the free stream fluid flow which is indicated by T_∞ and ignoring higher order terms, the T^4 can be defined as:

$$T^4 \cong -3T^4 + 4TT_\infty^3 \quad (5)$$

The specified boundary conditions are:

$$v = v_w;\ u = \lambda u_w + A\frac{\partial u}{\partial y};\ \ T = T_w + B\frac{\partial T}{\partial y};\ \text{at}\ y = 0$$

$$u \to 0;\ \ T \to T_\infty;\ \ \text{as}\ \ y \to \infty \quad (6)$$

where v, u are the velocity components in the x and y directions and U_∞ and u_w are the velocities of free stream fluid and sheet respectively, A and B are slip factors, T, μ_{nf} , α_{nf} and ρ_{nf} are the temperature, viscosity, thermal diffusivity and density of the nanofluid respectively, as defined in [32]:

$$\alpha_{nf} = \frac{k_{nf}}{(\rho c_p)_{nf}},\ \mu_{nf} = \frac{\mu_f}{(1-\phi)^{2.5}}$$

$$\rho_{nf} = (1-\phi)\rho_f + \phi\rho_s$$

$$\frac{k_{nf}}{k_f} = \frac{(2k_f+k_s)-(-k_s+k_f)2\phi}{(2k_f+k_s)+(-k_s+k_f)\phi}$$

$$(\rho c_p)_{nf} = (1-\phi)(\rho c_p)_f + \phi(\rho c_p)_s \quad (7)$$

where ρ_s and ρ_f are the densities of solid nanoparticles volume fractions and fluid (water) respectively, k_f and k_s are the thermal conductivities of the base fluid and solid nanoparticles volume fractions respectively. Furthermore, the μ_{nf} (the viscosity of the nanofluid) was estimated in [33] and the similarity transformation is taken according to [34]:

$$u = cxf'^{(\eta)};\ v = -\sqrt{c\vartheta}f(\eta);\ \ \eta = y\sqrt{\frac{c}{\vartheta_f}};$$

$$\theta(\eta) = \frac{T-T_\infty}{T_w-T_\infty} \quad (8)$$

Transformation (8) instantly fulfills the differentiation in terms of (1), however (2) and (3) are reduced to the following non-linear ordinary differential equations:

$$\frac{1}{(1-\phi)^{2.5}} f''' + \left((-\phi+1) + \phi\left(\rho_s/\rho_f\right)\right)\left(ff'' - f'^2\right) = 0 \quad (9)$$

$$\frac{1}{Pr}\frac{1}{\left((1-\phi)+\phi\left((\rho c_p)_s/(\rho c_p)_f\right)\right)}\left(\frac{k_{nf}}{k_f} + \frac{4}{3}Rd\right)\theta'' + f\theta' = 0 \quad (10)$$

and the boundary conditions take the form:

$$f(0) = S;\ f'(0) = \lambda + \delta f''(0);\ \theta(0) = 1 + \delta_T\theta'(0)$$
$$\text{at } \eta = 0,\ f'(\eta) \to 0;\ \theta(\eta) \to 0;\ \text{as } \eta \to \infty) \quad (11)$$

where prime stands for the derivative with respect to η, $Rd\left(= 4T_\infty^3\sigma^*/k^*{}_f k_f\right)$ is the radiative parameter, $Pr\ (= \mu_f\ /k_f\ )$ is the Prandtl number, $\delta = A\sqrt{c/\vartheta_f}$ is the velocity slip, $\delta_T = B\sqrt{c/\vartheta_f}$ is the thermal slip parameter and λ is the stretching/shrinking parameter. When $0 < \lambda < 1$, the fluid and the plate are moved in the similar direction. Likewise, for $\lambda < 0$ and $\lambda > 1$, these are in opposite direction of the motion. When $\lambda < 0$ shows that the flow of the ambient fluid is in the positive *x*-direction and the movement of sheet is in negative *x*-direction, $\lambda > 1$ shows that the flow of ambient fluid is in the negative *x*-direction and the movement of the sheet in the positive *x*-direction. In the present paper, both cases are considered but main focus was given on $\lambda < 0$.

The local Nusselt number Nu_x and the skin friction coefficient C_f are key physical parameters that are described as:

$$C_f = \frac{\tau_w}{\rho_f u_w{}^2},\ \ Nu_x = \frac{q_w}{k_f(T_w - T_\infty)} \quad (12)$$

Shear stress τ_w and surface heat diffusion q_w are defined as:

$$\tau_w = \mu_{nf}\left(\frac{\partial u}{\partial y}\right)_{y=0} \text{ and } q_w = -\left(\frac{k_{nf}}{k_f} + \frac{4}{3}Rd\right)\left(\frac{\partial T}{\partial y}\right)_{y=0} \quad (13)$$

By the use of (8) and (13) in (12), we get:

$$C_f(Re_x)^{\frac{1}{2}} = \frac{1}{(1-\phi)^{2.5}} f''(0)$$
$$(Re_x)^{-\frac{1}{2}} Nu_x = -\left(\frac{k_{nf}}{k_f} + \frac{4}{3}Rd\right)\theta'(0) \quad (14)$$

where $Re_x = \frac{xu_w}{\vartheta_f}$ reports the Reynolds number.

III. STABILITY ANALYSIS

As this problem has dual solutions, stability analysis is required to find a stable and physically reliable solution. To evaluate the stability of the solutions, at first the governing system of (2) and (3) will be written into an unsteady form like:

$$\frac{\partial u}{\partial t} + v\frac{\partial u}{\partial y} + u\frac{\partial u}{\partial x} = \frac{\mu_{nf}}{\rho_{nf}}\frac{\partial^2 u}{\partial y^2} \quad (15)$$

$$\frac{\partial T}{\partial t} + v\frac{\partial T}{\partial y} + u\frac{\partial T}{\partial x} = \frac{k_{nf}}{(\rho c_p)_{nf}}\left(1 + \frac{4Rd}{3}\right)\frac{\partial^2 T}{\partial y^2} \quad (16)$$

where t denotes the time. The transformation (8) will be modified by introducing new dimensionless time dependent variable τ.

$$u = cxf'^{(\eta,\tau)};\ v = -\sqrt{cx}f(\eta,\tau);$$
$$\eta = y\sqrt{\frac{c}{\vartheta_f}};\ \theta(\eta,\tau) = \frac{T-T_\infty}{T_w-T_\infty} \text{ and } \tau = ct \quad (17)$$

By implementing (17) into the (15) and (16) we get:

$$\frac{\partial^3 f(\eta,\tau)}{\partial\eta^3} + (-\phi+1)^{2.5}\left[\left((-\phi+1) + \phi\left(\rho_s/\rho_f\right)\right)\left\{\frac{1}{2}f(\eta,\tau)\frac{\partial^2 f(\eta,\tau)}{\partial\eta^2} - \left(\frac{\partial f(\eta,\tau)}{\partial\eta}\right)^2 - \frac{\partial^2 f(\eta,\tau)}{\partial\eta\partial\tau}\right\}\right] = 0 \quad (18)$$

$$\frac{1}{Pr}\left(\frac{k_{nf}}{k_f} + \frac{4Rd}{3}\right)\frac{\partial^2\theta(\eta,\tau)}{\partial\eta^2} + \left(1 - \phi + \phi\frac{(\rho c_p)_s}{(\rho c_p)_f}\right)\left[\frac{\partial\theta(\eta,\tau)}{\partial\eta}f(\eta,\tau) - \frac{\partial\theta(\eta,\tau)}{\partial\tau}\right] = 0 \quad (19)$$

The boundary conditions are:

$$f(0,\tau) = S\,, \frac{\partial f(0,\tau)}{\partial\eta} = \lambda + \delta\frac{\partial^2 f(0,\tau)}{\partial\eta^2},$$
$$\theta(0,\tau) = 1 + \delta_T\frac{\partial\theta(0,\tau)}{\partial\eta},$$
$$\frac{\partial f(\eta,\tau)}{\partial\eta} \to 0,\ \theta(\eta,\tau) \to 0 \text{ as } \eta \to \infty \quad (20)$$

To obtain stability for the solutions $f(\eta) = f_0(\eta)$ and $\theta(\eta) = \theta_0(\eta)$ that satisfy the specified boundary value problem given in equations (2)-(3), we expressed:

$$f(\eta,\tau) = F(\eta)e^{-\gamma\tau} + f_0(\eta),$$
$$\theta(\eta,\tau) = G(\eta)e^{-\gamma\tau} + \theta_0(\eta) \quad (21)$$

$G(\eta)$ and $F(\eta)$ are the related functions to $\theta_0(\eta)$ and $f_0(\eta)$ respectively, and γ is the unknown minimum eigenvalue. The following linear eigenvalue problem system is generated by using (19) into (18)-(21):

$$\frac{\partial^3 F}{\partial\eta^3} + (-\phi+1)^{2.5}\left[\left((-\phi+1) + \phi\left(\rho_s/\rho_f\right)\right)\left\{\frac{\partial^2 F}{\partial\eta^2}f_0 + F\frac{\partial^2 f_0}{\partial\eta^2} - 2\frac{\partial f}{\partial\eta}\frac{\partial F}{\partial\eta} + \gamma\frac{\partial F}{\partial\eta}\right\}\right] = 0 \quad (22)$$

$$\frac{1}{Pr}\left(\frac{k_{nf}}{k_f} + \frac{4Rd}{3}\right)\frac{\partial^2 G}{\partial\eta^2} + \left(1 - \phi + \phi\frac{(\rho c_p)_s}{(\rho c_p)_f}\right)\left[f_0\frac{\partial G}{\partial\eta} + \frac{\partial\theta_0}{\partial\eta}F + \gamma G\right] = 0 \quad (23)$$

The set $F(\eta) = F_0(\eta)$ and $G(\eta) = G_0(\eta)$ is used in (22) and (23) to acquire the initial decay or growth of solutions of (21). Therefore, the following system of eigenvalues has been solved:

$$F_0''' + (-\phi+1)^{2.5}\left\{\left((-\phi+1)+\phi\left(\frac{\rho_s}{\rho_f}\right)\right)(F_0''f_0 + \gamma F_0' - 2f_0'F_0' + f_0''F_0)\right\} = 0 \quad (24)$$

$$\frac{1}{Pr}\left(\frac{k_{nf}}{k_f}+\frac{4Rd}{3}\right)G_0'' + \left(1-\phi+\phi\frac{(\rho c_p)_s}{(\rho c_p)_f}\right)\{G_0'f_0 + \theta_0'F_0 + \gamma G_0\} = 0 \quad (25)$$

with boundary conditions:

$$F_0(0) = 0,\ F_0'(0) = \delta F_0''(0),\ G_0(0) = \delta_T G_0'(0)$$
$$F_0'(\eta) \to 0,\ G_0(\eta) \to 0 \text{ as } \eta \to \infty \quad (26)$$

To get the smallest eigenvalue, the linearized equations (24) and (25) with boundary conditions (26) are solved in MATLAB using the bvp4c solver techniques. As mentioned in [35], we must relax one boundary condition into the initial condition. In this case, $F_0{}'(\eta) \to 0$ as $\eta \to \infty$ into $F''_0(0) = 1$. The smallest negative eigenvalues indicate the disturbance's initial growth. As a result, the solutions related to the fluid flow are said to be unstable. The fluid flow is said to be stable in case obtained smallest positive eigenvalues.

IV. NUMERICAL METHOD

The boundary value problem given in (9) and (10) is solved using the shooting method in Maple software, using the initial and boundary conditions (11). On the other hand, this method turns the boundary value problem into an initial value problem. Therefore, we get:

$$f' = F_P, f'' = F_{PP}$$
$$\left(1+\frac{1}{\beta}\right)F_{PP}' + (1-\phi)^{2.5}\left\{\left(1-\phi+\phi\left(\frac{\rho_s}{\rho_f}\right)\right)(FF_{PP} - (F_P)^2)\right\} = 0 \quad (27)$$

$$\theta' = \theta_P, \phi' = \phi_P,$$

$$\frac{1}{Pr}\frac{1}{\left((1-\phi)+\phi\left((\rho c_p)_s/(\rho c_p)_f\right)\right)}\left(\frac{k_{nf}}{k_f}+\frac{4}{3}Rd\right)\theta_P' + F\theta_P = 0 \quad (28)$$

The boundary conditions take the form:

$$F(0) = S, F_P(0) = \lambda + \delta F_{PP}(0), \theta(0) = 1 + \delta_T\theta_P(0)$$
$$F_{PP}(0) = \alpha_1, \theta_P(0) = \alpha_2, \quad (29)$$

where α_1, α_2 are taken as the unknown initial conditions. So, the shooting values for the missing initial values of α_1, α_2 are important. The solution must satisfy the boundary conditions $F_P(\eta) \to 0, \theta(\eta) \to 0$ as $\eta \to \infty$ of the specified boundary value problem. The computation is done in Maple by using the shootlib function and the shooting method. In this paper, the thickness of the boundary layer η_∞ is taken between 4 and 7, at which the convergence shown in the graphs is obtained. For fixed values of the used parameters, 2 velocity and temperature profiles are achieved, each totally satisfying the problem's required boundary conditions. As a result, the quantities $f''(0)$ and $-\theta'(0)$, have two distinct values.

V. RESULTS AND DISCUSSION

The shooting method in Maple is used to obtain the numerical solutions to the system of ordinary differential equations (9) and (10) that are subjects to the boundary conditions of (11). Figures 2–17 show the results of the impact of the non-dimensional physical parameters on the velocity and temperatures profiles as well as the skin friction coefficient and Nusselt numbers. Table I shows the thermo physical properties of the base fluid and nanoparticles used in the present study. Table II shows the comparison result of the 2 numerical methods, the shooting method used in Maple and the bvp4c used in Matlab. The comparison shows much symmetry in the results that encourage us to consider that our obtained results are correct and trustworthy. In addition, in the case of dual solutions, stability analysis has been performed with bvp4c in Matlab to determine which solution is reliable and stable by obtaining the smallest eigenvalue using (24)-(26). The solution which corresponds to a positive least eigenvalue is considered as a reliable and stable solution. The solution which corresponds to a negative least eigenvalue is considered as an unstable solution. Table III shows the numerical values of the stability of solutions for the different values of velocity slip and radiation. The eigenvalues (γ) concerned to the second solutions are negative, while they are positive for the first solutions. The results of Fe_2O_3-water base nanofluid and Fe-water base nanofluid are shown by different colors in plots. The solid lines are related to the study of the stable solution (first solution) and the dashed lines are used to denote the second, unstable solutions. Table IV shows the critical points concerned to Figures 2-5, where two solutions are merged. Furthermore, the impact of the various used parameters of this study are presented and discussed below through graphs.

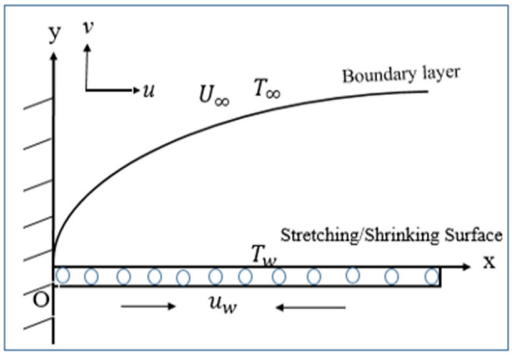

Fig. 1. Physical illustration of the model.

The variation in skin friction coefficient (f "(0)) and local Nusselt number ($-\theta'(0)$) along the change in stretching and shrinking parameter (λ) under the impact of different values of the suction parameter (S) are shown in Figures 2 and 3 respectively. For $\lambda > \lambda_c$, there are dual solutions. Both solutions merge at λ_c, and there is no solution for $\lambda < \lambda_c$ where λ_c denotes the critical point. Figure 2 shows that when the suction rate is increased, the skin friction coefficient reduces for values $\lambda > 0$ and rises for $\lambda < 0$ in the first (stable) solution. Furthermore, the rate of skin friction (drag force) is examined to be larger in Fe_2O_3-water base nanofluid than in

Fe-water base nanofluid for $\lambda > 0$ (for stretching case of the sheet) and vice versa for $\lambda < 0$ (for shrinking case of the sheet) for the same values of the suction parameter (S). The Nusselt number (rate of heat transfer) rises as the suction parameter (S) is increased in both solutions (Figure 3).

In addition, the variations of skin friction coefficient ($f''(0)$) and local Nusselt number ($-\theta'(0)$) along the variation of the suction parameter at various values of nanoparticles volume fraction (ϕ) are shown in Figures 4-5. For $S > S_c$, dual solutions also exist. At the critical point S_c, both solutions merge, while no solution is observed for $S < S_c$. In both Fe_2O_3-water base and Fe-water base nanofluids, the skin friction coefficient rises as the nanoparticle volume fraction increases, while it decreases in the second solution (Figure 4). The rate of skin friction for the Fe-water base nanofluid is observed to be greater than that of the Fe_2O_3-water base nanofluid. It may be noted that the viscous fluid flow in Figures 4 and 5 is shown by black colored lines. Figure 5 shows that the Nusselt number decreases with an increase in the rate of nanoparticles volume fraction in both solutions in both types of nanofluids. Heat transfer rate is observed greater in Fe-water base nanofluid than in Fe_2O_3-water base nanofluid. The comparative results of the variations of the skin friction coefficient and local Nusselt number with the variation of nanoparticles volume fraction regarding to Fe_2O_3-water base nanofluid and Fe-water base nanofluid are presented in Figures 6 and 7. It is seen that the Fe-nanoparticles show the greater resistance in flow, which means greater rate of skin friction coefficient is observed as compared to the Fe_2O_3 in water base nanofluid. Due to the greater resistance of suspending Fe nanoparticles in water, the rate of heat transfer of Fe-water base nanofluid remains greater than that of the Fe_2O_3-water base nanofluid as shown in Figure 7. Furthermore, due to the repeated trend of the result, only graphs of Fe-water base nanofluid are presented here for further study.

Furthermore, Figures 8-17 show the velocity and temperature profiles for various values of the applied parameters. Figures 8 and 9 show the velocity and the temperature profiles of the boundary layer flow of the Fe-water base nanofluid at different values of nanoparticle volume fraction (ϕ). The influence of ϕ shows that with any increment in the concentration of nanoparticles the velocity of the fluid decreases throughout the boundary layer region in the first (stable) solution. Actually, the nanoparticles develop a friction in fluid molecules which retards the flow. The nanoparticles also increase the thermal conductivity of the base fluid, so the heat is transferred from the hot regime to the cold one in faster rate and in result, warms the thermal boundary layer regime. Hence, the concentration of nanoparticles increases the temperature and the thermal boundary layer thickness of the base fluid as shown in Figure 9. The effects of the suction parameter (S) on $f'(\eta)$ and $\theta(\eta)$ profiles are shown in Figures 10 and 11. It can be clearly observed that any increment in S raises the suction rate of the fluid at sheet and in result, momentum boundary layer thickness and fluid velocity decrease in the first solution throughout the nanofluid flow. In the second solution, the opposite result can be observed. Any increment in S decreases the thermal boundary layer thickness and the temperature of the nanofluid throughout the flow in both solutions. Figures 12 and 13 show the impact of λ (for shrinking case) on $f'(\eta)$ and $\theta(\eta)$ profiles respectively. Both the profiles of velocity $f'(\eta)$ and temperature $\theta(\eta)$ are decreasing for increasing λ (in the first solution) and increasing for increasing λ (in the second solution) for the shrinking case.

The influence of the Prandtl number (Pr) on the temperature profile $\theta(\eta)$ of the Fe-water base nanofluid is shown in Figure 14. When the parameter Pr is raised, the temperature of the nanofluid decreases. Because fluids with a high Pr value have a low thermal diffusivity, the temperature of the moving fluid drops. The temperature and thickness of the boundary layer decrease as Pr increases. The influence of radiation parameter (Rd) on the temperature profile is drawn in Figure 15. The temperature profile increases as the radiation parameter increases. As the value of Rd increases, the divergence of radiating heat flux increases as k^* decreases. As a consequence, the rate of radiating heat transfer to the fluid's boundary layer flow rises which increases the temperature of the fluid. The velocity profile $f'(\eta)$ of the Fe-water base nanofluid in the first solution decreases when the velocity slip parameter (δ) increases, as can be seen in Figure 16. Basically, any increment in δ shows more fluid particles slipping on sheet, so the fluid flow decelerates near the sheet. In the second solution, any change in parameter values causes the nanofluid velocity to rise. The influence of thermal slip parameter (δ_T) on the temperature profile $\theta(\eta)$ is shown in Figure 17. When the thermal slip increases, the thickness of the thermal boundary layer and the temperature profile both decrease in both solutions. The fluid velocity is initially decreased when the thermal slip parameter is raised, resulting in a decrease in net molecular mobility. Consequently, less molecular momentum decreases the thermal boundary layer thickness and the temperature profile.

VI. CONCLUSION

The steady two-dimensional boundary layer flow and heat transfer of Fe_2O_3 and Fe-water base nanofluid over a flat stretching/shrinking sheet with radiation and slip effects were studied numerically in this paper. The nanofluid model in [7] is used with a porous medium. The similarity transformation is used to convert the system of partial differential equations into ordinary differential equations. The shooting method is used to solve these equations numerically. Due to the existence of dual solutions, stability analysis is performed using bvp4c in Matlab. The following conclusions are drawn based on the numerical investigations:

- Dual solutions are observed for certain ranges of stretching/shrinking and suction parameters.
- Stability analysis shows that one solution is stable and physically reliable while the other is unstable.
- The skin friction coefficient decreases for $\lambda > 0$ and increases for $\lambda < 0$ as the rate of suction is increased.
- The heat transfer rate and the skin friction coefficient are decreasing in the second solution when the velocity slip parameter δ increases.

- Fe-water nanofluid shows a greater rate of skin friction and Nusselt number as compared to Fe_2O_3-water nanofluid.
- An increase in nanoparticles' volume fraction decreases the skin friction coefficient and increases the Nusselt number.
- Increase in velocity slip, suction, nanoparticles volume fraction, and shrinking parameters decreases the velocity profiles and the associated boundary layers thicknesses.
- The rise in nanoparticle volumetric fraction and radiation increases the temperature profiles and the boundary layer thicknesses.

TABLE II. COMPARISON ALONG THE VARIATION OF $f''(0)$, AND $-\theta'(0)$ WITH λ AT $s = 2$, $Pr = 6.2$, $\delta = 0.1, \phi = 0.1$, $\delta_T = 0.7$ AND $Rd = 1.5$ FOR FE-WATER BASE NANOFLUID

Parameter λ	Shooting method		bvp4c method	
	$f''(0)$	$-\theta'(0)$	$f''(0)$	$-\theta'(0)$
-1	1.2976198	0.83568	1.297520	0.83667
-0.6	0.919529	0.59991	0.919595	0.598838
0	0.00000	0.88279	0.00000	0.883671
0.5	-0.92239	0.8969	-0.92356	0.89789
1	-1.69817	0.90856	-1.69773	0.90891

TABLE III. SMALLEST EIGENVALUES AGAINST VARIOUS δ AND Rd VALUES WHEN $\delta_T = 0.7, \phi = 0.1, \lambda = -1, S = 2$ AND $Pr = 6.2$ FOR FE-WATER BASE NANOFLUID

Parameters		bvp4c method	
δ	Rd	1st solution	2nd solution
0.2	0.5	0.83568	-1.297520
0.2	1	0.59991	-0.919595
0.3	0.3	0.88279	-0.00000
0.4	0.6	0.8969	-0.92356

TABLE IV. CRITICAL POINT VALUES OF THE INVESTIGATED NANOFLUIDS

Parameters	Numerical values	Critical point (Fe)	Critical point (Fe_2O_3)
S	2	-1.552	-1.1675
	2.15	-1.811	-1.357
	2.3	-2.092	-1.565
ϕ	0	1.9096	1.9096
	0.1	1.666	1.825
	0.2	1.625	1.859

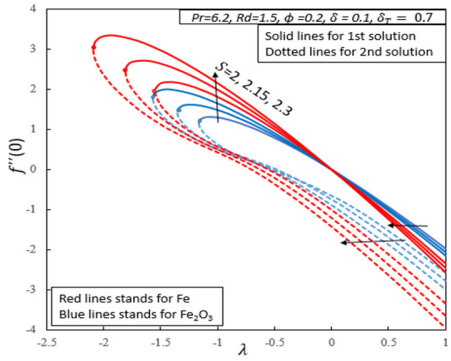

Fig. 2. Skin-friction $f''(0)$ variation against various λ and S values.

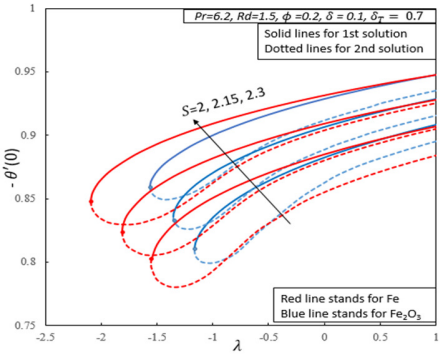

Fig. 3. Nusselt number against various λ and S values.

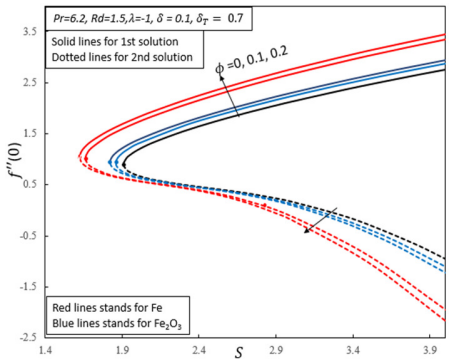

Fig. 4. Skin-friction against various S and ϕ values.

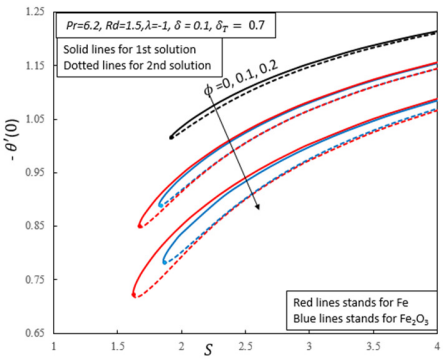

Fig. 5. Nusselt number against various S and ϕ values.

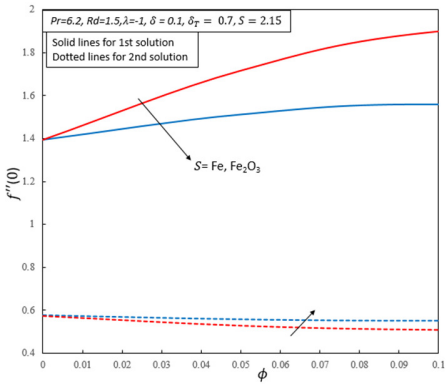

Fig. 6. Skin-friction against ϕ for the particular nanoparticles in water base nanofluid.

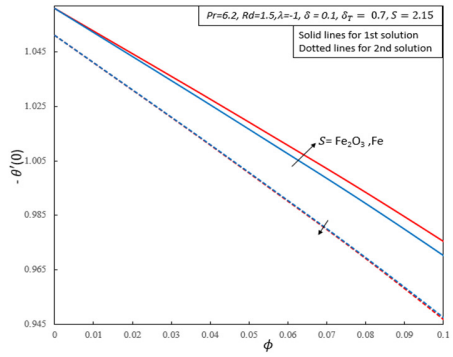

Fig. 7. Nusselt number against ϕ for particular nanoparticles in water base nanofluid.

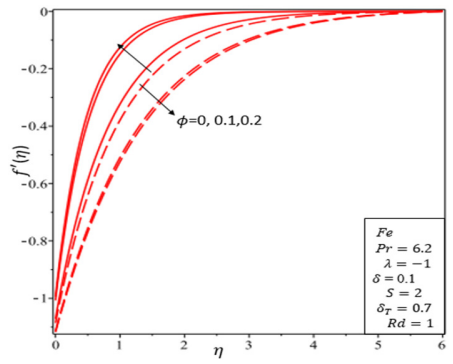

Fig. 8. Velocity $f'(\eta)$ against various ϕ values.

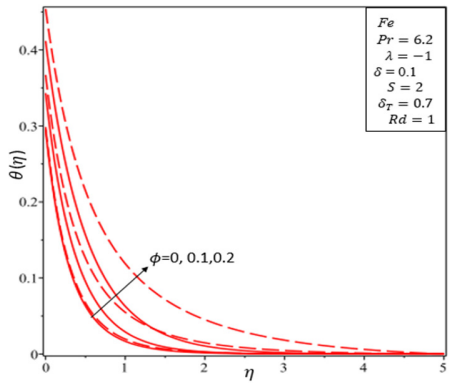

Fig. 9. Temperature $\theta(\eta)$ against various ϕ values.

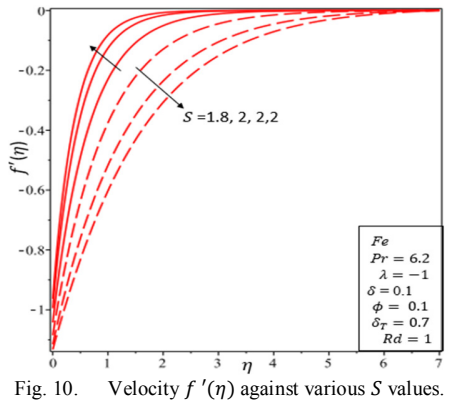

Fig. 10. Velocity $f'(\eta)$ against various S values.

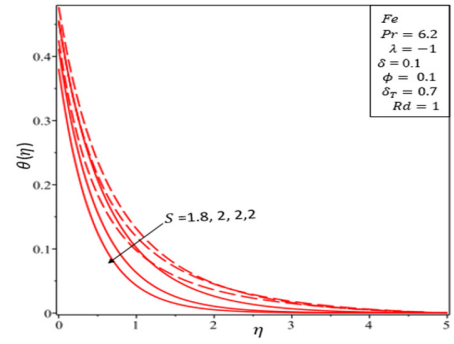

Fig. 11. Temperature $\theta(\eta)$ against various S values.

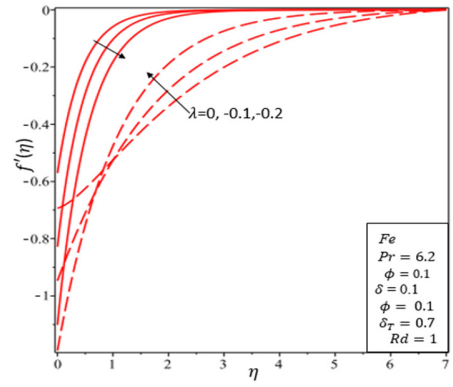

Fig. 12. Velocity $f'(\eta)$ against various λ values.

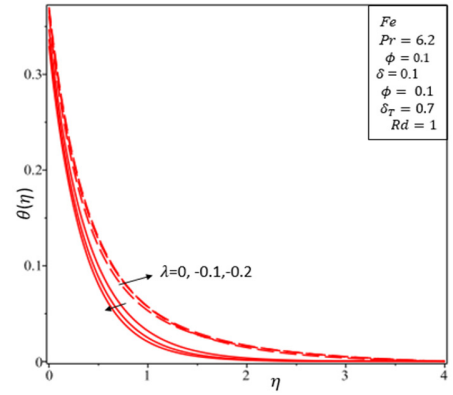

Fig. 13. Temperature $\theta(\eta)$ against various λ values.

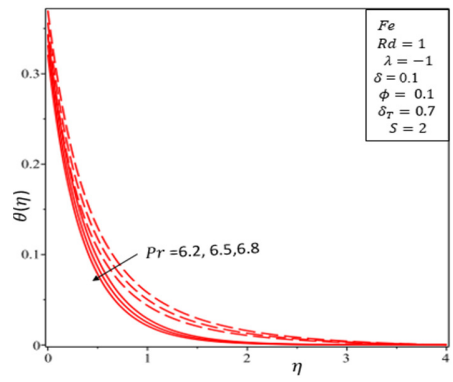

Fig. 14. Temperature $\theta(\eta)$ against various Pr values.

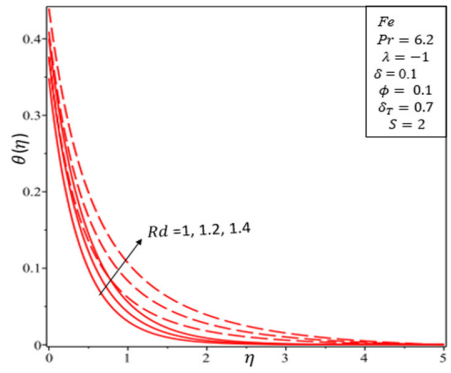

Fig. 15. Temperature $\theta(\eta)$ against various Rd values.

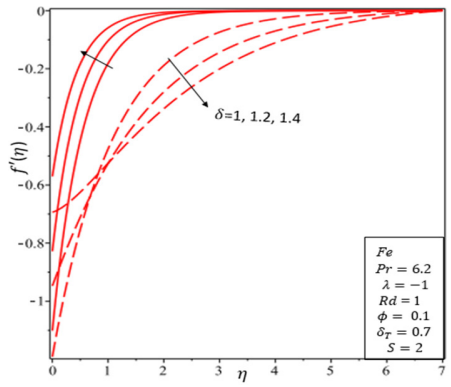

Fig. 16. Velocity $f'(\eta)$ against various δ values.

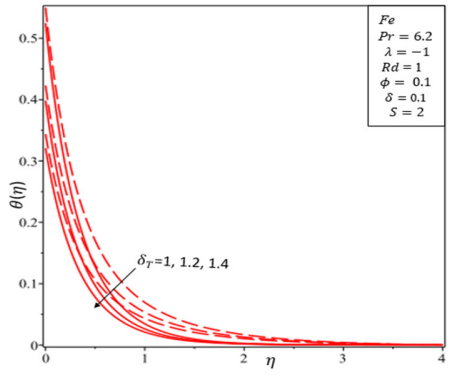

Fig. 17. Temperature $\theta(\eta)$ against various δ_T values.

ACKNOWLEDGMENT

The authors are indebted to their institutes for facilitating this research. The authors declare no conflict of interest.

REFERENCES

[1] S. U. S. Choi and J. A. Eastman, "Enhancing thermal conductivity of fluids with nanoparticles," in *International Mechanical Engineering Congress and Exhibition*, San Francisco, CA, USA, Nov. 1995.

[2] M. S. Abel, P. L. Rao, and J. V. Tawade, "The effect of magnetic field on the boundary layer flow over a stretching sheet in a nanofluid with convective boundary condition," *International Journal of Mechanical Engineering and Technology*, vol. 6, no. 4, pp. 87–100, 2015.

[3] K. Boukerma and M. Kadja, "Convective Heat Transfer of Al2O3 and CuO Nanofluids Using Various Mixtures of Water-Ethylene Glycol as Base Fluids," *Engineering, Technology & Applied Science Research*, vol. 7, no. 2, pp. 1496–1503, Apr. 2017, https://doi.org/10.48084/etasr.1051.

[4] A. Latreche and M. Djezzar, "Numerical Study of Natural Convective Heat and Mass Transfer in an Inclined Porous Media," *Engineering, Technology & Applied Science Research*, vol. 8, no. 4, pp. 3223–3227, Aug. 2018, https://doi.org/10.48084/etasr.2179.

[5] F. Z. Mecieb, F. G. Bermejo, J. P. S. Fernández, and S. Laouedj, "Convective Heat Transfer During Melting in a Solar LHTES," *Engineering, Technology & Applied Science Research*, vol. 11, no. 3, pp. 7181–7186, Jun. 2021, https://doi.org/10.48084/etasr.4165.

[6] J. Buongiorno, "Convective Transport in Nanofluids," *Journal of Heat Transfer*, vol. 128, no. 3, pp. 240–250, Aug. 2005, https://doi.org/10.1115/1.2150834.

[7] R. K. Tiwari and M. K. Das, "Heat transfer augmentation in a two-sided lid-driven differentially heated square cavity utilizing nanofluids," *International Journal of Heat and Mass Transfer*, vol. 50, no. 9, pp. 2002–2018, May 2007, https://doi.org/10.1016/j.ijheatmasstransfer.2006.09.034.

[8] A. Mohd Rohni, S. Ahmad, and I. Pop, "Boundary layer flow over a moving surface in a nanofluid beneath a uniform free stream," *International Journal of Numerical Methods for Heat & Fluid Flow*, vol. 21, no. 7, pp. 828–846, Jan. 2011, https://doi.org/10.1108/09615531111162819.

[9] L. A. Lund, Z. Omar, I. Khan, and S. Dero, "Multiple solutions of Cu-C6H9NaO7 and Ag-C6H9NaO7 nanofluids flow over nonlinear shrinking surface," *Journal of Central South University*, vol. 26, no. 5, pp. 1283–1293, May 2019, https://doi.org/10.1007/s11771-019-4087-6.

[10] S. Dero, A. M. Rohni, and A. Saaban, "MHD Micropolar Nanofluid Flow over an Exponentially Stretching/Shrinking Surface: Triple Solutions," *Journal of Advanced Research in Fluid Mechanics and Thermal Sciences*, vol. 56, no. 2, pp. 165–174, 2019.

[11] M. Anwar, K. Rafique, M. Misiran, and I. Khan, "Numerical Solution of Casson Nanofluid Flow Over a Non-linear Inclined Surface With Soret and Dufour Effects by Keller-Box Method," *Frontiers in Physics*, vol. 7, 2019, Art. no. 139, https://doi.org/10.3389/fphy.2019.00139.

[12] L. J. Crane, "Flow past a stretching plate," *Zeitschrift fur Angewandte Mathematik und Physik ZAMP*, vol. 21, no. 4, pp. 645–647, Jul. 1970, https://doi.org/10.1007/BF01587695.

[13] P. S. Gupta and A. S. Gupta, "Heat and mass transfer on a stretching sheet with suction or blowing," *The Canadian Journal of Chemical Engineering*, vol. 55, no. 6, pp. 744–746, 1977, https://doi.org/10.1002/cjce.5450550619.

[14] M. Miklavcic and C. Wang, "Viscous flow due to a shrinking sheet," *Quarterly of Applied Mathematics*, vol. 64, no. 2, pp. 283–290, Apr. 2006, https://doi.org/10.1090/S0033-569X-06-01002-5.

[15] T. Hayat, Z. Abbas, and M. Sajid, "On the Analytic Solution of Magnetohydrodynamic Flow of a Second Grade Fluid Over a Shrinking Sheet," *Journal of Applied Mechanics*, vol. 74, no. 6, pp. 1165–1171, Jan. 2007, https://doi.org/10.1115/1.2723820.

[16] M. Sajid, T. Javed, and T. Hayat, "MHD rotating flow of a viscous fluid over a shrinking surface," *Nonlinear Dynamics*, vol. 51, no. 1, pp. 259–265, Jan. 2008, https://doi.org/10.1007/s11071-007-9208-3.

[17] W. A. Khan and I. Pop, "Boundary-layer flow of a nanofluid past a stretching sheet," *International Journal of Heat and Mass Transfer*, vol. 53, no. 11, pp. 2477–2483, May 2010, https://doi.org/10.1016/j.ijheatmasstransfer.2010.01.032.

[18] C. Y. Wang, "Flow due to a stretching boundary with partial slip—an exact solution of the Navier–Stokes equations," *Chemical Engineering Science*, vol. 57, no. 17, pp. 3745–3747, Sep. 2002, https://doi.org/10.1016/S0009-2509(02)00267-1.

[19] F. Mabood, W. A. Khan, and A. I. M. Ismail, "MHD boundary layer flow and heat transfer of nanofluids over a nonlinear stretching sheet: A numerical study," *Journal of Magnetism and Magnetic Materials*, vol. 374, pp. 569–576, Jan. 2015, https://doi.org/10.1016/j.jmmm.2014.09.013.

[20] T.-P. Teng, Y.-H. Hung, T.-C. Teng, H.-E. Mo, and H.-G. Hsu, "The effect of alumina/water nanofluid particle size on thermal conductivity,"

Applied Thermal Engineering, vol. 30, no. 14, pp. 2213–2218, Oct. 2010, https://doi.org/10.1016/j.applthermaleng.2010.05.036.

[21] A. M. Rohni, S. Ahmad, A. I. Md. Ismail, and I. Pop, "Boundary layer flow and heat transfer over an exponentially shrinking vertical sheet with suction," *International Journal of Thermal Sciences*, vol. 64, pp. 264–272, Feb. 2013, https://doi.org/10.1016/j.ijthermalsci.2012.08.016.

[22] N. S. Anuar, N. Bachok, and I. Pop, "A Stability Analysis of Solutions in Boundary Layer Flow and Heat Transfer of Carbon Nanotubes over a Moving Plate with Slip Effect," *Energies*, vol. 11, no. 12, Dec. 2018, Art. no. 3243, https://doi.org/10.3390/en11123243.

[23] M. A. A. Hamad and I. Pop, "Scaling Transformations for Boundary Layer Flow near the Stagnation-Point on a Heated Permeable Stretching Surface in a Porous Medium Saturated with a Nanofluid and Heat Generation/Absorption Effects," *Transport in Porous Media*, vol. 87, no. 1, pp. 25–39, Mar. 2011, https://doi.org/10.1007/s11242-010-9683-8.

[24] M. Turkyilmazoglu, "Fully developed slip flow in a concentric annuli via single and dual phase nanofluids models," *Computer Methods and Programs in Biomedicine*, vol. 179, Oct. 2019, Art. no. 104997, https://doi.org/10.1016/j.cmpb.2019.104997.

[25] S.-R. Yan, M. Izadi, M. A. Sheremet, I. Pop, H. F. Oztop, and M. Afrand, "Inclined Lorentz force impact on convective-radiative heat exchange of micropolar nanofluid inside a porous enclosure with tilted elliptical heater," *International Communications in Heat and Mass Transfer*, vol. 117, Oct. 2020, Art. no. 104762, https://doi.org/10.1016/j.icheatmasstransfer.2020.104762.

[26] S. Dero, A. Mohd Rohni, and A. Saaban, "Effects of the viscous dissipation and chemical reaction on Casson nanofluid flow over the permeable stretching/shrinking sheet," *Heat Transfer*, vol. 49, no. 4, pp. 1736–1755, 2020, https://doi.org/10.1002/htj.21688.

[27] S. Dero, A. M. Rohni, and A. Saaban, "Stability analysis of Cu−C6H9NaO7 and Ag−C6H9NaO7 nanofluids with effect of viscous dissipation over stretching and shrinking surfaces using a single phase model," *Heliyon*, vol. 6, no. 3, Mar. 2020, Art. no. e03510, https://doi.org/10.1016/j.heliyon.2020.e03510.

[28] J. H. Merkin, "On dual solutions occurring in mixed convection in a porous medium," *Journal of Engineering Mathematics*, vol. 20, no. 2, pp. 171–179, Jun. 1986, https://doi.org/10.1007/BF00042775.

[29] A. Ishak, "Dual Solutions in Mixed Convection Boundary Layer Flow: A Stability Analysis," *International Journal of Mathematical, Computational, Physical and Quantum Engineering*, vol. 8, no. 9, pp. 1160–1163, Aug. 2014.

[30] P. D. Weidman, D. G. Kubitschek, and A. M. J. Davis, "The effect of transpiration on self-similar boundary layer flow over moving surfaces," *International Journal of Engineering Science*, vol. 44, no. 11, pp. 730–737, Jul. 2006, https://doi.org/10.1016/j.ijengsci.2006.04.005.

[31] K. Merrill, M. Beauchesne, J. Previte, J. Paullet, and P. Weidman, "Final steady flow near a stagnation point on a vertical surface in a porous medium," *International Journal of Heat and Mass Transfer*, vol. 49, no. 23, pp. 4681–4686, Nov. 2006, https://doi.org/10.1016/j.ijheatmass transfer.2006.02.056.

[32] N. Najib, N. Bachok, and N. M. Arifin, "Stability of Dual Solutions in Boundary Layer Flow and Heat Transfer over an Exponentially Shrinking Cylinder," *Indian Journal of Science and Technology*, vol. 9, Jan. 2017, Art. no. 48, https://doi.org/10.17485/ijst/2016/v9i48/135911.

[33] H. C. Brinkman, "The Viscosity of Concentrated Suspensions and Solutions," *The Journal of Chemical Physics*, vol. 20, no. 4, pp. 571–571, Apr. 1952, https://doi.org/10.1063/1.1700493.

[34] R. Sharma, A. Ishak, and I. Pop, "Partial Slip Flow and Heat Transfer over a Stretching Sheet in a Nanofluid," *Mathematical Problems in Engineering*, vol. 2013, Apr. 2013, Art. no. e724547, https://doi.org/10.1155/2013/724547.

[35] S. D. Harris, D. B. Ingham, and I. Pop, "Mixed Convection Boundary-Layer Flow Near the Stagnation Point on a Vertical Surface in a Porous Medium: Brinkman Model with Slip," *Transport in Porous Media*, vol. 77, no. 2, pp. 267–285, Mar. 2009, https://doi.org/10.1007/s11242-008-9309-6.

[36] W. N. Mutuku-Njane, "Analysis of hydromagnetic boundary layer flow and heat transfer of nanofluids," Ph.D. dissertation, Cape Peninsula University of Technology, Cape Town, South Africa, 2014.